

# Two tonoplast proton pumps function in Arabidopsis embryo development

Yu-Tong Jiang<sup>1</sup>, Ren-Jie Tang<sup>2</sup>, Yan-Jie Zhang<sup>1</sup>, Hong-Wei Xue<sup>3,4</sup> , Ali Ferjani<sup>5</sup> , Sheng Luan<sup>2\*</sup>  and Wen-Hui Lin<sup>1,2\*</sup> 

<sup>1</sup>School of Life Sciences and Biotechnology, The Joint International Research Laboratory of Metabolic & Developmental Sciences, Shanghai Jiao Tong University, 200240, Shanghai, China;

<sup>2</sup>Department of Plant and Microbial Biology, University of California, Berkeley, CA 94720, USA; <sup>3</sup>School of Agriculture and Biology, Shanghai Jiao Tong University, 800 Dongchuan Road, Shanghai 200240, China; <sup>4</sup>National Key Laboratory of Plant Molecular Genetics, CAS Center for Excellence in Molecular Plant Sciences, Institute of Plant Physiology and Ecology, Chinese Academy of Sciences, 200032, Shanghai, China; <sup>5</sup>Department of Biology, Tokyo Gakugei University, 184-8501, Koganei-shi, Japan

## Summary

Authors for correspondence:

Wen-Hui Lin

Tel: +86 21 34208262

Email: whlin@sjtu.edu.cn

Sheng Luan

Tel: +1 510 642 6306

Email: sluan@berkeley.edu

Received: 30 May 2019

Accepted: 22 September 2019

New Phytologist (2020) 225: 1606–1617

doi: 10.1111/nph.16231

**Key words:** auxin, cotyledons, vacuole, V-ATPase, V-PPase.

- Two types of tonoplast proton pumps, H<sup>+</sup>-pyrophosphatase (V-PPase) and the H<sup>+</sup>-ATPase (V-ATPase), establish the proton gradient that powers molecular traffic across the tonoplast thereby facilitating turgor regulation and nutrient homeostasis. However, how proton pumps regulate development remains unclear.
- In this study, we investigated the function of two types of proton pumps in Arabidopsis embryo development and pattern formation. While disruption of either V-PPase or V-ATPase had no obvious effect on plant embryo development, knocking out both resulted in severe defects in embryo pattern formation from the early stage.
- While the first division in wild-type zygote was asymmetrical, a nearly symmetrical division occurred in the mutant, followed by abnormal pattern formation at all stages of embryo development. The embryonic defects were accompanied by dramatic differences in vacuole morphology and distribution, as well as disturbed localisation of PIN1. The development of mutant cotyledons and root, and the auxin response of mutant seedlings supported the hypothesis that mutants lacking tonoplast proton pumps were defective in auxin transport and distribution.
- Taking together, we proposed that two tonoplast proton pumps are required for vacuole morphology and PIN1 localisation, thereby controlling vacuole and auxin-related developmental processes in Arabidopsis embryos and seedlings.

## Introduction

Vacuoles play a central role in plant growth and development. They are lytic compartments as well as primary reservoirs for nutrients and metabolites. The central vacuole in a mature plant cell is held together by a membrane referred to as a tonoplast. Arrays of transport proteins reside in the tonoplast to transport ions and solutes inside and outside the vacuole to maintain a proper turgor pressure and nutrient homeostasis of the cell. Molecular fluxes across the tonoplast are mainly energised by two types of primary proton pumps, the vacuolar H<sup>+</sup>-ATPase (V-ATPase) and the vacuolar H<sup>+</sup>-pyrophosphatase (V-PPase) (Neuhaus & Trentmann, 2014). These two redundant proteins cooperate to generate the membrane potential and proton gradient across the tonoplast essential for secondary transport processes. In Arabidopsis, there are three genes encoding H<sup>+</sup>-pyrophosphatase that are divided into type I (AVP1/ATVHP1;1/

FUGU5) and type II (AVP2;1 and AVP2;2) (Drozdowicz & Rea, 2001). Among these genes, only type I (AVP1/ATVHP1;1/ FUGU5, AT1G15690) is located in the tonoplast (Gaxiola *et al.*, 2001; Maeshima, 2001; Segami *et al.*, 2010). Genetic analysis of Arabidopsis *avp1* mutants suggested that AVP1 plays a role in several physiological processes such as seedling growth, gluconeogenesis and high magnesium tolerance, which may mainly contribute to its pyrophosphatase activity but be independent of H<sup>+</sup>-translocation (Ferjani *et al.*, 2011; Yang *et al.*, 2018). A recent study supported the idea that AVP1 and V-ATPase both contribute to vacuolar acidification in Arabidopsis (Kriegel *et al.*, 2015). V-ATPases are multisubunit proton pumps comprised of the peripheral V<sub>1</sub> complex responsible for ATP hydrolysis and the integral membrane V<sub>0</sub> complex in charge of proton translocation (Nishi & Forgac, 2002; Sze *et al.*, 2002; Nelson, 2003; Cipriano *et al.*, 2008). In plant cells, V-ATPases are not only found in the tonoplast but also present in the *trans*-Golgi network/early endosome (TGN/EE) (Herman *et al.*, 1994; Oberbeck *et al.*, 1994). Three distinct isoforms of the V<sub>0</sub> subunit (including VHA-

\*These authors contributed equally in this work.

a1,2,3) are encoded in the Arabidopsis genome and two of these, VHA-a2 (AT2G21410) and VHA-a3 (AT4G39080), are exclusively targeted to the tonoplast, whereas VHA-a1 (AT2G28520) only resides in the TGN/EEs and the deletion mutant of *VHA-a1* is lethal (Dettmer *et al.*, 2006). Therefore, the Arabidopsis *vha-a2 vha-a3* double mutant that lacks both tonoplast-localised  $V_0$  isoforms should be null in tonoplast V-ATPase function (Krebs *et al.*, 2010). Interestingly, in contrast with the *vha-a1* single mutant that is lethal, the *vha-a2 vha-a3* double mutant remains viable and developmentally normal although it is stunted in growth possibly due to defects in nutrient homeostasis (Krebs *et al.*, 2010). More surprisingly, the triple mutant, *vha-a2 vha-a3 avp1* lacking both tonoplast V-ATPase and V-PPase activities, is viable and retains some vacuolar acidification capacity, suggesting that other players may additively contribute to the pH gradient across the tonoplast (Kriegel *et al.*, 2015).

During the initial phase of functional analysis of AVP1, a study linked AVP1 function with auxin-regulated plant development (Li *et al.*, 2005). However, a later study (Kriegel *et al.*, 2015) demonstrated that the mutant *avp1-1* used in Li *et al.* (2005) contained a mutation in *GNOM* (Steinmann *et al.*, 1999; Geldner *et al.*, 2001) gene, leading to the observed auxin-related phenotypes. During our study on the functional relationship of AVP1 and V-ATPase, we also confirmed that the *avp1* single mutant failed to show auxin-related defects. However, we discovered that when both AVP1 and V-ATPase were disrupted, the mutant plants showed severe defects in auxin-regulated developmental processes. In our study, a series of previously unreported phenotypes in the *vha-a2 vha-a3 avp1* triple mutant was identified that were clearly connected to vacuole morphology and auxin signalling in the context of plant embryogenesis and development. Two different alleles lacking both tonoplast V-ATPase and V-PPase (from this point forward the *vha-a2 vha-a3 avp1* allele is designated as *vap3* and the *vha-a2 vha-a3 fugu5-1* allele is designated as *fap3*), but not any single or double mutants, displayed severe growth defects in embryo development and seedling establishment. The defects in the triple mutants lacking both pumps were reminiscent of those observed in mutants defective in auxin transport or signalling. Indeed, further experiments using various transgenic auxin marker lines suggested that those auxin-related developmental phenotypes were correlated with the impairment in overall auxin level, auxin polar transport and distribution. In particular, the key auxin exporter PIN1 was misregulated in the mutants at multiple levels including protein abundance, exocytosis and polar localisation, and this could account for the severe defects in embryo pattern formation, seedling development and auxin responses in the mutants. Taken together, our results linked the function of vacuolar proton pumps to auxin-regulated developmental processes.

## Materials and Methods

### Plant materials and growth conditions

All Arabidopsis plants were grown in soil under glasshouse conditions (22°C; 16 h : 8 h, light : dark cycle for long day) or on half-

strength Murashige and Skoog ( $\frac{1}{2}$ MS) medium (Murashige & Skoog, 1962) containing 2% sucrose and 0.75% agar in a growth chamber (22°C : 18°C, 16 h : 8 h, light : dark cycle). The wild-type control used in this study was Col-0 ecotype and all of our plant materials were on the Col-0 background. The *avp1* mutant corresponded to the T-DNA insertion line GK-596F06-025557 from the Luan laboratory (Yang *et al.*, 2015). Primers for genotyping were: AVP1-747F, 5'-TGGGATCTACACTAAGGCTGCTG-3' and AVP1-1268R, 5'-CCATAATGAGTCCAGCCCAAAG-3'. The primers for genotyping the mutation site in *fugu5-1*: forward, 5'-CAGGCTGGTGTATCAGAGCAT-3' and reverse, 5'-GACTCAACAGCCATGAGCTT-3'. The *vha2* mutant was constructed using two T-DNA insertion lines *vha-a2* (SALK\_142642) and *vha-a3* (SALK\_029786) from Salk Institute for Biological Studies, and identified by genotyping (primers: VHA-a2-LP, 5'-GCAACTCGTTCAAGTCATTG-3' and VHA-a2-RP 5'-ACCGCTGCAA CTTGTCGTTA-3'; VHA-a3-LP 5'-CGATGGATCTGATGCGTTCAG-3' and VHA-a3-RP 5'-AGCATGAATGTACCTGTGCTG-3'). Transgenic lines: *pPIN1::PIN1-EYFP* (Xu *et al.*, 2006) and DR5::GUS (Sabatini *et al.*, 1999) were obtained from the Ben Scheres laboratory. We crossed these two marker lines with mutants *avp1*, *vha2* and *vap3* and named these PIN1-EYFP *avp1*, PIN1-EYFP *vha2*, PIN1-EYFP *vap3* and DR5::GUS *avp1*, DR5::GUS *vha2* and DR5::GUS *vap3*.

### Root gravitropism assay

Sterilised seeds were sown on  $\frac{1}{2}$ MS medium containing 2% sucrose. The 7 d after germination (DAG) seedlings of similar size (average root length) were transferred to  $\frac{1}{2}$ MS medium containing 2% (w/v) sucrose and 0.85% agar. The position of the root apex was marked on the back of the plates, and then the plates were rotated by 90° for gravitropism assay. Images were captured every 2 h by digital camera (Canon D60, EF-S 18-135mm f/3.5-5.6 IS STM, Taiwan, China). IMAGEJ was used (<http://rsbweb.nih.gov/ij/download.html>) to analyse the tip angle (the angle between root tips and the horizontal direction).

### Chemical treatment

The 5-DAG-seedlings were transplanted to vertical plates with  $\frac{1}{2}$ MS medium containing 0.1  $\mu$ M or 0.5  $\mu$ M 1-naphthylacetic acid (NAA; Sigma 317918) and 10  $\mu$ M *N*-(1-naphthyl)phthalamic acid (NPA; Sigma 399728). The 5-DAG-seedlings were vacuum fixed (0.5 MPa pressure for 30 min) in 4% polyoxymethylene (PFA; Sigma 158127) solution. After washing three times with PBS solution (NaCl 8 g, KCl 0.2 g, Na<sub>2</sub>HPO<sub>4</sub> 1.42 g, KH<sub>2</sub>PO<sub>4</sub> 0.27 g, 1 l, pH 7.4), the seedlings were cleared into Clearsee solution, which was prepared as described by Kurihara *et al.* (2015). BCECF/AM was used as the staining agent to visualise vacuole morphology and to measure vacuolar pH, as previously described (Viotti *et al.*, 2013).

### Histological and fluorescence staining

The root staining experiment required applying vacuum for 3 min for roots in 4% paraformaldehyde (PFA) solution diluted

with PBS (containing 1% Triton X-100). Fluorescent Brightener 28 (FB28; Sigma F3543) was used as a staining agent for root cell walls, and was diluted in 2% (w/v) Clearsee solution. After 3 min staining, roots were washed in Clearsee solution three times and sealed under coverslips.  $\beta$ -Glucuronidase (GUS) activity was detected by histochemical staining of tissues at 37°C for 6 h and bleaching with 75% alcohol. GUS-stained cotyledons were examined under a stereomicroscope (Leica S8APO, Wetzlar, Germany) and digital images were captured using a Leica DFC450 microscope. Brefeldin A (BFA; Sigma 203729) treatment was performed in conjunction with FM4-64 (Sigma F34653) staining. After incubation in FM4-64 solution (4  $\mu$ M in  $\frac{1}{2}$ MS liquid medium) for 5 min, 5-DAG-seedlings were carefully washed in  $\frac{1}{2}$ MS liquid medium with tweezers for three times, the seedlings were immersed in BFA treatment solution (50  $\mu$ M in  $\frac{1}{2}$ MS liquid medium) for 50 min before observation. The process of confocal laser scanning microscopy (CLSM) was to drawn from a paper by Christensen and colleagues (Christensen *et al.*, 1997). We dissected the pistils by first removing the sepals, petals and stamens from isolated flowers. Then we cut the stigma of pistils use a needle in a millilitre syringe under the stereoscope and gently drew two scratches on pistil walls. The pistils were immersed in a solution of 4% glutaraldehyde and 12.5 mM cocodylate for at least 4 h after applying a vacuum for 45 min. Then the tissue was dehydrated in 10%, 30%, 50%, 70%, 80%, 90% and 95% ethanol for 10 min each. After immersion in 95% ethanol for 12 h, the tissue was cleared in a 2 : 1 mixture of benzyl benzoate : benzyl alcohol for 2 h. Then seeds were peeled out of the pistils and soaked in Leica Immersion oil 11513859 for 2 h and finally sealed under coverslips.

### Confocal imaging

Embryos for fluorescence observation were separated from siliques at each developmental stage. The root we observed were separated from 5-DAG seedlings, which were grown vertically in  $\frac{1}{2}$ MS medium with 2% sucrose. Samples were fixed, cleaned and dyed. Then images were captured using a confocal microscope (Leica/ TCS SP8 STED 3X) with a  $\times 63$  magnification oil objective. For detection of PIN1-EYFP, excitation wavelength was set at 515 nm and emission wavelength was between 525 and 575 nm. For detection of FB28 staining, excitation wavelength was set at 405 nm and emission wavelength was between 450 and 500 nm. For detection of CLSM staining, excitation wavelength was 488 nm and the emission wavelength was between 525 and 555 nm. The intensity of the argon ion laser was 8% and laser intensity is 50 in Leica LAS AF LITE software (en.freedownloadmanager.org/Windows-PC/Leica-LAS-AF-Lite-FREE.html). Fluorescence intensity statistics were calculated using IMAGEJ software (<http://rsbweb.nih.gov/ij/download.html>).

### Scanning electron microscopy

For embryo observation, we soaked the dried seeds for 20 min and carefully peeled the seed coats with tweezers. For seedling cotyledon observation, we use 6 DAG seedlings. Samples were fixed in FAA solution (anhydrous ethanol : 37%

formaldehyde : glacial acetic acid : distilled water, 10 : 2 : 1 : 7, v/v/v/v) at 0.6 MPa pressure for 20 min. The materials were sealed and stored at 4°C for 7 d before gradient alcohol dehydration (50%, 60%, 70%, 80%, 90%, 95% and 100% C<sub>2</sub>H<sub>5</sub>OH; each concentration was applied for 15 min, the last 100% concentration was repeated three times). After drying using an Automated Critical Point Dryer (Leica/CPD 300, Wetzlar, Germany), the materials were coated with gold particles for 20 min. Coated samples were transferred to a scanning electron microscope (Hitachi/S3400II, Tokyo, Japan) for examination.

### Vacuole extraction

We used rosette leaves of 35 DAG seedlings as the material for extracting the vacuoles. Next, 1 g fresh rosette leaves were taken and sliced into 2 mm pieces using a razor blade. Our method of vacuole extraction was the same as described in a previous paper (Robert *et al.*, 2007). We extracted the protoplasts with protoplast enzyme solution and washed these gently with wash buffer. The protoplasts were disrupted using prewarmed lysis buffer and the vacuoles could be inspected under a Leica DFC450 microscope. The vacuole solution was overlaid with 3 ml 4% Ficoll solution and 1 ml ice-cold vacuole buffer. After spinning for 50 min at 71 000 *g* at 10°C, vacuoles should be visible with between 0 and 4% Ficoll.

### Real-time quantitative RT-PCR

To detect the transcription levels of *AVP1*, *VHA-a2*, *VHA-a3* and *CUC* genes in Col and *vap3* seedlings, cotyledons of 5 DAG seedlings were collected and total RNA was extracted using TRIzol reagent (Invitrogen 10296010), and then RNA was reverse transcribed using the FastKing RT Kit (with gDNase) (Tiagen KR116, Beijing, China). The primers used for qRT-PCR were as follows. *AVP1*: forward, 5'-CTGTCATTGCTGATAATGTCCG-3' and reverse, 5'-GATTCCCATTGAACTGATGAGC-3'. *VHA-a2*: forward, 5'-GCAACATCTTCATACGACAGTC-3' and reverse, 5'-ACCTGAAACCTCAGTCATCATT-3'. *VHA-a3*: forward, 5'-CATGCTTAGTCTTGATGTGACG-3' and reverse, 5'-ACTCTTTGGTTCTTAGGACCTG-3'. The *ACTIN2* gene was used as a positive internal control with the following primers: forward, 5'-CCTTCGTCCTTGATCTTGCGG-3' and reverse, 5'-AGCGATGGCTGGAACAGAAC-3'. Quantitative RT-PCR was conducted using the Eppendorf realplex 4s cyclor and the SYBR<sup>®</sup> Green Real-time PCR Master Mix (Thermo Fisher Scientific, Waltham, MA, USA) and analysed using the threshold cycle (CT) method.

### SDS-PAGE and immunoblotting

Roots from 6 DAG seedlings were used, and the roots were cut to a uniform height with scissors. PIN1 protein was analysed using SDS-PAGE and subsequent immunoblotting. After gel electrophoresis, the proteins were transferred to a nitrocellulose membrane (Whatman, Buckinghamshire, UK). The primary antibodies against PIN1 and TUBULIN A was obtained from Abmart (Berkeley Heights, NJ, USA). Secondary antibodies for

PIN1 were antirabbit IgG (Abmart) and secondary antibodies for TUBULIN A were antimouse IgG (H + L) (Abmart). Immunostained bands were analysed using a charge coupled device (CCD) camera system (Bio-Rad).

### Phytohormone targeted metabolome analysis

This experiment used the UPLC-ESI-MS/MS analysis method to qualitatively detect auxin in samples. We took 2 g fresh leaves from 21 DAG seedling rosette leaves and lyophilised these using a lyophiliser (Labconco & Scientz-10N, Ningbo, China). Then 500 µl treatment solution was added (isopropyl alcohol : water : FA, 2 : 1 : 0.002) in 14 mg lyophilised sample, which was ground with two steel balls (one large and one small) for 2 min. After incubating at  $-20^{\circ}\text{C}$  for 20 min, the samples were treated with ultrasound in an ice bath for 30 min and 1 ml chloroform was added. After another  $-20^{\circ}\text{C}$  incubation for 20 min, samples were treated with ultrasound in an ice bath for 5 min and then centrifuged at 15 871 *g* for 5 min before vortexing for 1 min. Then, 900 µl of the lower layer was removed (divided into two tubes, each 450 µl) in a 1.5 ml brown liquid chromatography mass spectrometry (LCMS) sample vial and the samples were dried. Samples were resuspended in 200 µl treatment solution (methanol : water, 4 : 1) with ultrasound treatment in an ice bath for 1 min. Samples were stored at  $-20^{\circ}\text{C}$  before being placed in the machine (the whole process being at low temperature). An API 5500 Triple Quadrupole Mass Spectrometry System from AB Sciex, with an electrospray (ESI) ion source and an Analyst 1.6.2 workstation (Redwood City, CA, USA) were used. The Waters ultra-high performance liquid chromatograph with an Agilent Poroshell 120, EC-C18 (100 × 3 mm, 2.7 m) liquid chromatography (LC) column (Shanghai, China) was used based on auxin; injection volume was 3 µl. Default parameters were used for the ANALYST software (v.1.6.2; AB Sciex) to automatically identify and integrate each multi reaction monitoring transition and assist with manual inspection.

## Results

### Tonoplast proton pumps play an essential role in embryogenesis

Triple mutants were constructed lacking both V-ATPase (VHA-a2 and VHA-a3) and V-PPase (AVP1) to investigate the function of tonoplast proton pumps in Arabidopsis. We first crossed two single mutants of *VHA-a2* (SALK\_142642) and *VHA-a3* (SALK\_029786) to generate the double mutant *vha2*, which had the same genotype as a previously reported mutant (Krebs *et al.*, 2010), but was remade by our group. This double mutant was further crossed, respectively, with two different alleles of the *AVP1* gene, *avp1* (Yang *et al.*, 2015) and *fugu5-1* (Ferjani *et al.*, 2007) to produce two triple mutants *vap3* and *fap3* (Supporting Information Fig. S1a,b). *fap3* has the same genotype as a mutant described previously (Kriegel *et al.*, 2015) but was remade by our group and *vap3* was a new triple mutant allele. These triple mutants were confirmed using PCR and qRT-PCR (Fig. S1c, d).

Phenotypic analysis illustrated that *vap3* and *fap3* went through an abnormal embryogenesis. We examined embryo development of Col and *vap3* and found that 70% of *vap3* ovules failed to develop to the 1-cell embryo and the others embryos showed various degree of abnormal pattern formation (Fig. 1a–u). The embryos of *vap3* had an abnormal embryonic body and abnormal suspensor, as well as stunted or arrested development (Fig. 1v). The embryo development of *fap3* had similar defects as found for *vap3* (Fig. 1v). Microscope analysis of *vap3* mutant embryos at the 1-cell stage revealed defects from the very beginning of embryogenesis. The wild-type embryo contained a round apical cell and a long basal cell after the first horizontal and asymmetrical division. The apical cell was small with a thick cytoplasm and eventually developed to the embryo; the basal cell was larger and ultimately developed to the suspensor (Mayer *et al.*, 1993). The *vap3* and *fap3* embryo was defective throughout development from the 1-cell to 16-cell stages, and subsequently changed from globular heart-shaped at the maturation stage (Fig. 1a–u). Starting from the early stage, the suspensor cells were shorter and the cell division in some cases was arrested in *vap3* embryos (Fig. 1a–u). At the octant stage, the *vap3* embryo displayed multinuclear cells and unequal cytoplasmic division (Fig. 1g–i). From the globular to the heart-shaped stage, symmetrical primordia and intermediate boundaries of the cotyledons were established in the Col embryo, setting the foundation for cotyledon pattern formation (Long *et al.*, 1996). In *vap3* embryos, the cotyledon primordia became asymmetric with delayed cell division (Fig. 1n, o). We also observed embryogenesis and vacuole morphology in Col, *avp1* and *vha2* embryos (Fig. S2). Embryo development of wild-type and *avp1* embryos was not abnormal from the 1-cell embryo, while a relatively low proportion of *vha2* embryos had abnormal suspensors (Fig. 1v). Very few double mutants (2/187) showed abnormal cell division in the late stage of globular embryos (Fig. S2), and these had abnormal cotyledons after germination. Abnormal cell division and pattern formation in triple mutant embryos is summarised (Fig. 1w).

### Vacuole morphology and distribution were severely defective during embryogenesis in mutants lacking tonoplast proton pumps

A recent study (Kimata *et al.*, 2019) suggested that vacuole polar distribution plays an essential role in the first asymmetrical division of zygotes. Kriegel *et al.* (2015) reported that lack of two tonoplast proton pumps may have altered vacuole morphology in the elongation and transition zone of the mutant roots. Taking these studies together, we hypothesised that early embryonic cells in the *fap3* and *vap3* mutants may have altered vacuole morphology that leads to abnormal embryo pattern formation. Using CLSM and differential interference contrast (DIC) microscopy, we observed severe defects in the size, shape and distribution of vacuoles in mutant embryo cells compared with the wild-type (Figs 1a–c, 2). After the first division of the zygote in wild-type plants, a large vacuole was found in the basal cell, while the apical embryonic cell had very small vacuoles (Kimata *et al.*, 2019; Figs 1a, 2a). By contrast, at the same stage in triple mutants, apical

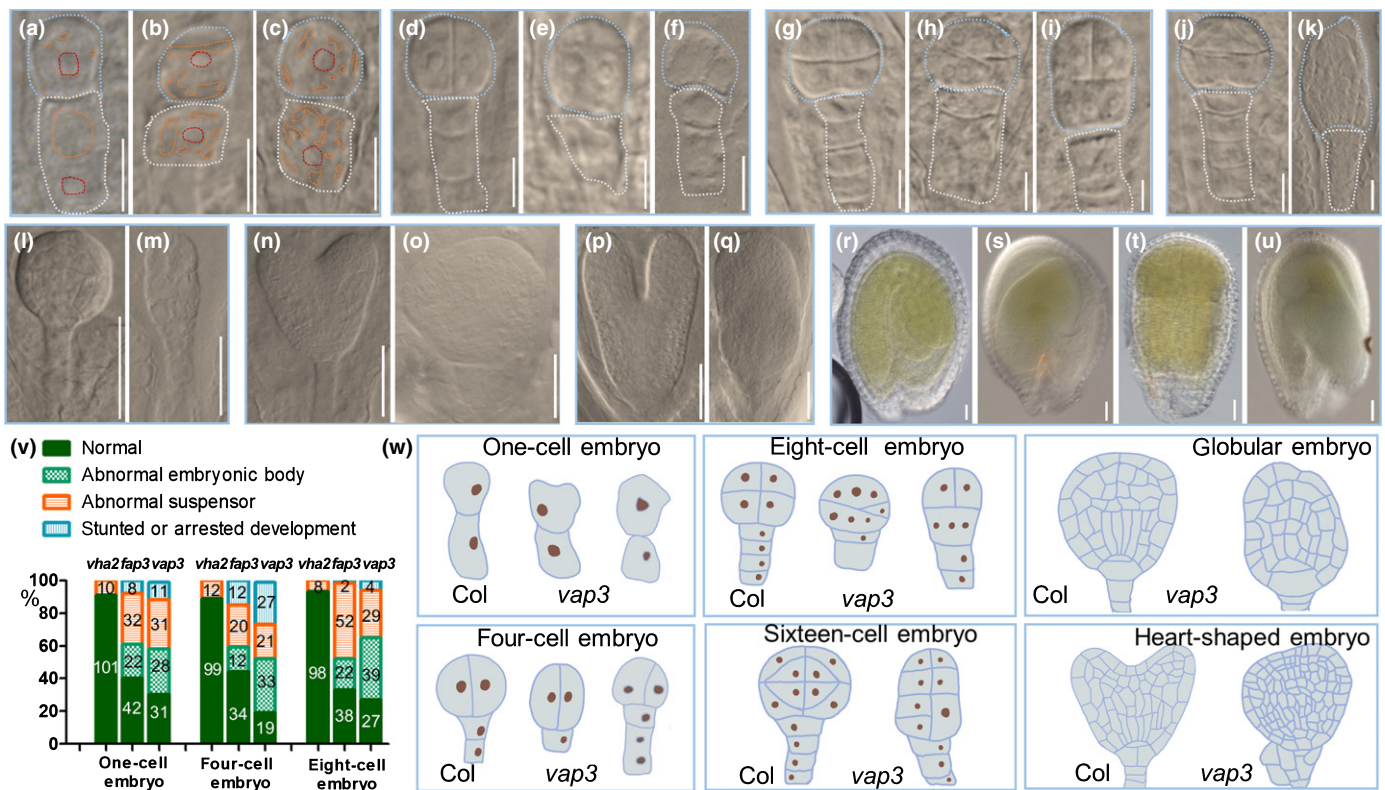


**Fig. 1** Abnormal embryogenesis of Arabidopsis mutant *vap3*. (a–k) One-cell, 4-cell, 8-cell and 16-cell embryos of Col (a, d, g, j) and *vap3* (b, c, e, f, h, i, k) (bars, 10  $\mu$ m). Blue lines indicate embryos, white lines indicate suspensors, red lines indicate nuclei of embryo cells, and orange lines indicate vacuoles. (l–q) Globular, heart-shaped, and torpedo-shaped embryos of Col (l, n, p) and *vap3* (m, o, q) (bars, 50  $\mu$ m). (r–u) Cotyledon embryos of Col (r) and *vap3* (s–u) (bars, 50  $\mu$ m). Graphs represent the typical phenotype of all samples ( $n = 100$  in each developmental stage of each line). (v) Phenotypic analysis of abnormal pattern formations in embryos of Col, *avp1*, *fugu5-1*, *vha2*, *vap3*, *fap3*. Sample numbers are labeled in each column. (w) The illustration of abnormal pattern formation of *vap3* embryos. Schematic diagrams of 1-cell to heart-shaped embryos showed the abnormal embryonic body and suspensor, which could be traced to (a–o).

cells featured larger vacuoles and the basal cells had many smaller vacuoles (Figs 1b, c, 2b). Subsequently, at the 4-, 8- and 16-cell embryo stages, larger vacuoles persisted in the embryo cells, whereas smaller vacuoles were found in suspensor cells in the mutant, accompanied by severe defects in cell division and pattern formation throughout these stages (Fig. 2c–i). As shown in Fig. 2(j), using a cartoon sketch, we aligned vacuole morphology and embryo cell division patterns. It was clear that abnormal vacuole morphology and distribution were tightly linked to defective embryo cell division and pattern formation. Together with another recent report (Kimata *et al.*, 2019), our results indicated that abnormal vacuole morphology was caused by defects in embryo cell division and pattern formation.

### Lacking tonoplast proton pump activity results in severe defects in plant morphogenesis

We compared the phenotypes of Col, *avp1*, *fugu5-1*, *vha2*, *vap3* and *fap3* plants during their life cycles and found very little difference in morphology between the single mutants and the wild-type. *vap3*, *fap3* and *vha2*, however, showed strong phenotypic changes compared with the wild-type or single mutant plants. Adult plants of the *vha2*, *vap3* and *fap3* mutants showed severely stunted stature and reproductive defects (Fig. S3). Furthermore,

we found new phenotypic defects in the triple mutants during early seedling development that had not been reported previously. In particular, almost all (99%) of *vap3* seedlings showed different degrees of cotyledon abnormality (Fig. 3a–m), including deformed two cotyledons, three cotyledons, partially fused cotyledons, and cup-shaped cotyledons (Fig. 3e–h). Another allele, *fap3*, produced 90% abnormal cotyledons (Fig. 3i–l). Compared with the triple mutants, a small proportion (less 1%) of *vha2* seedlings after germination had obvious abnormal cotyledons (mainly fused cotyledons) (Fig. 3d). Using a scanning electron microscope, we also found abnormal development of the shoot apical meristem (SAM) in *vap3* embryos, in addition to cotyledon defects (Fig. 3n– $\alpha$ ).

Consistent with the description of *fap3* mutants in a previous report (Kriegel *et al.*, 2015), the *vap3* and *fap3* seedlings displayed a short root phenotype compared with Col, *avp1*, and *fugu5-1* seedlings (Fig. 4a, b). We further examined the root tip anatomy of the *vap3* mutant and found a disturbed quiescent centre region and a smaller root cap, indicating an altered cell division pattern in the root meristem (Fig. 4c–n) and root cap (Fig. 4o). We also noted that the V-ATPase double mutant *vha2* showed reduced root growth, but *avp1* and *fugu5-1* mutants did not show any significant changes in pattern formation. Therefore, the two tonoplast proton pumps, AVP1 and V-ATPase, may

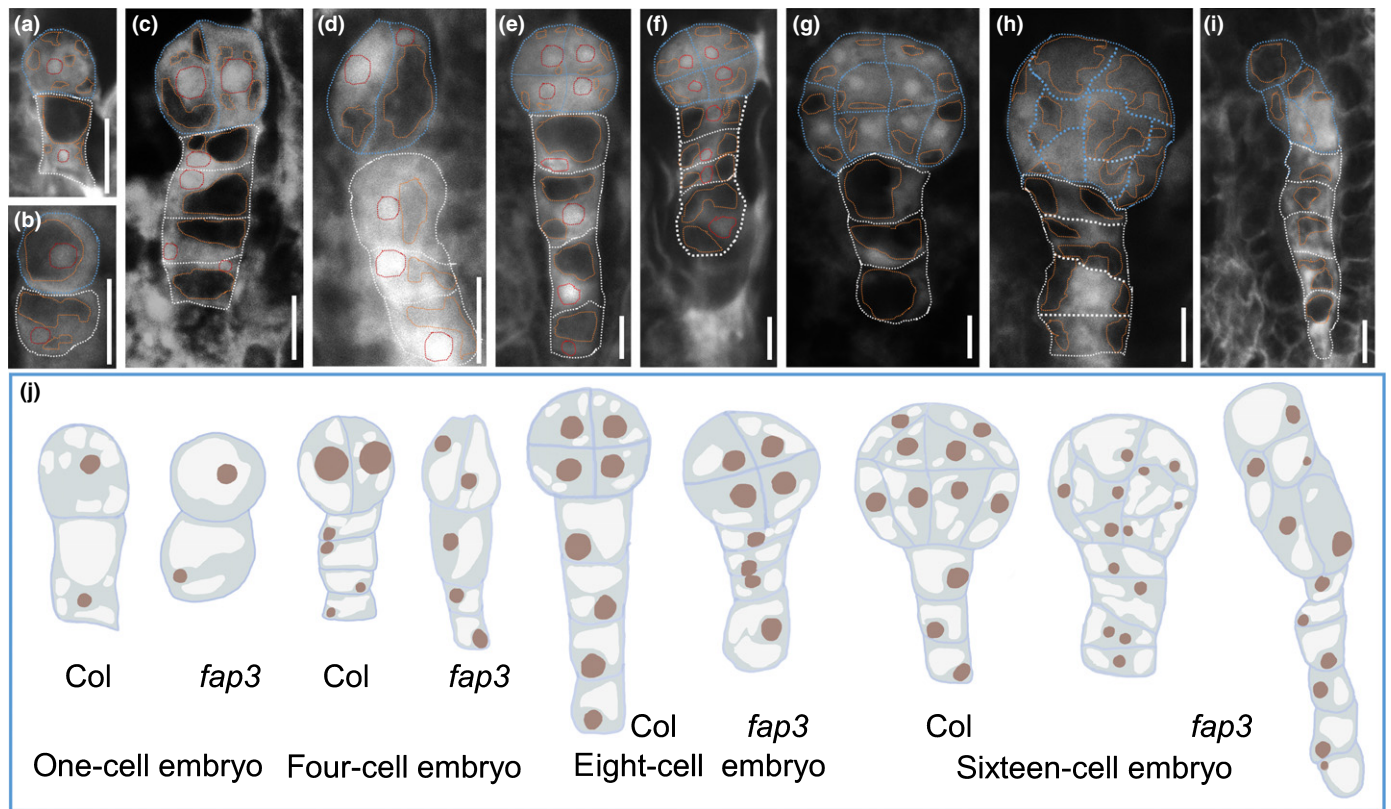


**Fig. 2** Abnormal vacuole morphology and distribution of Arabidopsis mutant *fap3*. (a, b) One-cell embryo of Col (a) and *fap3* (b). Bars, 10  $\mu$ m. (c–i) 4-cell, 8-cell, and 16-cell embryos of Col (c, e, g) and *fap3* (d, f, h, i) (bars, 10  $\mu$ m). Graphs represent the typical phenotype of all samples ( $n = 20$  in each developmental stage of Col and *fap3*). (j) Illustration of abnormal vacuole morphology and distribution of *fap3* embryos. (a–i) Blue lines indicate embryo cells, white lines indicate suspensor cells, red lines indicate nuclei of embryo cells, and orange lines indicate vacuoles. Schematic diagrams of 1-cell to 16-cell embryos showed the abnormal embryonic body and suspensor, which could be traced to (a–i).

have synergistic functions in the regulation of early plant pattern formation.

In addition to defects in root growth, the triple mutants *vap3* and *fap3* showed reduced gravity responses (Fig. S4a, b). Furthermore, *vap3/fap3* mutants were less sensitive to exogenous 1-naphthylacetic acid (NAA) (Fig. S4c). When treated with the auxin polar transport inhibitor NPA, *vha2*, *vap3* and *fap3* were less sensitive to NPA compared with the wild-type and single mutants, implying that auxin polar transport may be affected by disruption of the vacuolar proton pumps (Fig. S4d). Together, embryo defects and reduced auxin responses supported the hypothesis that the lack of vacuolar proton pumps may have altered auxin signalling in the mutant plants.

### PIN1 localisation and auxin distribution were altered in triple mutants

Pattern formation during embryogenesis, especially cotyledon initiation and development, is determined by auxin signalling (Galweiler *et al.*, 1998). Auxin signalling in plant development is often determined by the accumulation and transport of this hormone within plant organs, and is limited by the activities of several distinct families of transporters. In particular, PIN-FORMED (PIN) members play critical roles in polar auxin transport during embryonic and postembryonic stages, therefore tightly controlling plant

organogenesis and seedling development. Among the PINs, PIN1 is a major transporter for polar auxin flow during embryogenesis (Vernoux *et al.*, 2000). Cotyledon morphology at the mature stage of the *fap3* and *vap3* embryos, including fused cotyledons, multiple cotyledons, and asymmetric cotyledons (Figs 3a–m, S5a), is highly similar to that in the *pin1-11* mutant (Fig. S5b). We therefore crossed the PIN1-EYFP marker line with our mutants and compared its localisation in the wild-type and mutant backgrounds. In the wild-type embryos, the PIN1-EYFP signal appeared in the plasma membranes of 16-/32-cell embryos, and were localised in the vascular precursor cells and epidermal cell layer of cotyledon primordia after the late globular stage (Fig. 5a–d, Friml *et al.*, 2003; Xiang & Datla, 2011). In the mutant background, the PIN1-EYFP signal was reduced in intensity in 16-/32-cell embryos and heart-shaped embryos, and showed more diffused distribution in torpedo-shaped embryos and cotyledons (Fig. 5e–h). Furthermore, we found that PIN1 is mainly distributed in the basal side of the plasma membrane in root pericycle cells of wild-type plants (Fig. 5i–j). Interestingly, the PIN1 protein level was dramatically reduced in the *vap3* root (Fig. 5k, l). Western blot and fluorescence intensity of PIN1 in roots were produced to further demonstrate the reduction of total PIN1 protein in *vha2* and *vap3* (Fig. 5m–o).

We further examined auxin distribution and the accumulation pattern using transgenic plants expressing the  $\beta$ -glucuronidase

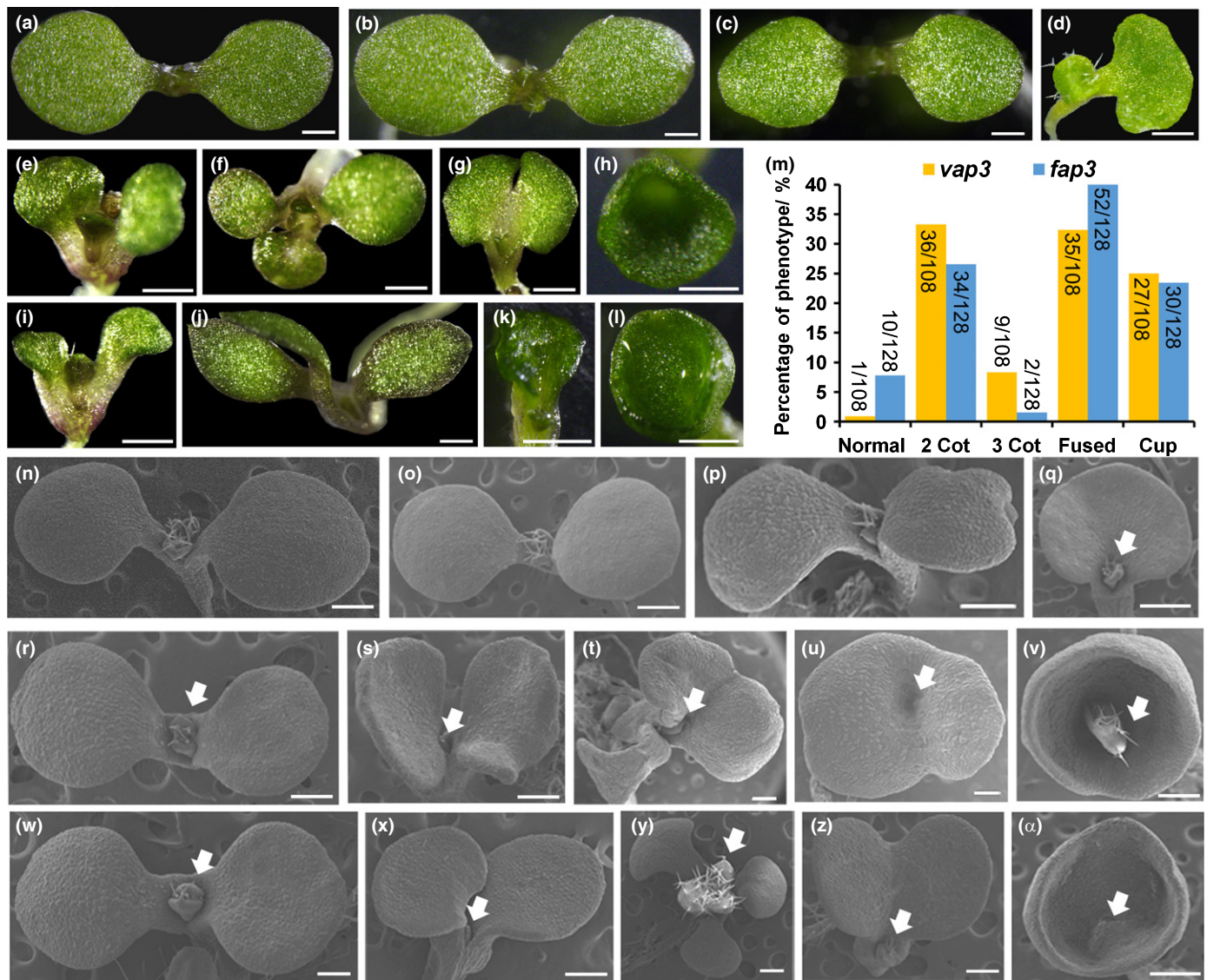


**Fig. 3** Abnormal cotyledons morphology in *Arabidopsis* mutants *vap3/fap3*. Cotyledons of Col (a), *avp1* (b), *fugu5-1* (c), *vha2* (d), *vap3* (e–h), and *fap3* (i–l) seedlings at 6 d after germination (DAG) (bars, 500  $\mu$ m). (m) Phenotypic analysis of different cotyledon phenotypes of *vap3* and *fap3*. 2 Cot represent abnormal two cotyledons, 3 Cot represent abnormal three cotyledons, fused represent partially fused cotyledon, cup represent cup-shaped cotyledon. Sample numbers are labelled in each column. Shoot apical meristems (SAM) in (n) Col, (o) *avp1*, (p) *fugu5-1*, (q) *vha2*, (r–v) *vap3*, (w–x) *fap3* (bars, 500  $\mu$ m). Arrows mark the SAM of seedlings. Graphs represent the typical phenotype of all samples ( $n = 100$  for each line).

(GUS) reporter gene driven by the synthetic auxin-responsive promoter DR5. Previous reports (Gonzalez *et al.*, 2010; Li *et al.*, 2010) have shown that auxin content is increased in transgenic lines overexpressing *AVP1*, indicating that *AVP1* activity is positively correlated with auxin content. We found that the GUS signal in the *avp1* mutant (Fig. S5c–f) was less intense compared with that in the wild-type, suggesting a disturbed auxin distribution in *avp1*. We measured the auxin content of young rosette leaves in 21-DAG *avp1* plants and indeed found a 32% drop in the auxin level compared with the wild-type (Table S1). In addition, we also found that distribution of the GUS signal was altered in *vha2* (Fig. S5e) and auxin content was also decreased in *vha2* (Table S1), suggesting that auxin content and polar transport were affected in *vha2* embryos. In the *vap3* triple mutant, the DR5 signal was less intense, the distribution of DR5 signal

was significantly changed (Fig. S5f), and auxin content decreased (Table S1), suggesting that both auxin content and distribution were affected in the triple mutant.

To investigate the detailed abnormality of mutant roots, we further visualised vacuole morphology in the two developmental zones. Roots were stained with FB28 (Fig. 6a), FM4-64 and BCECF-AM (Fig. 6b–e). In the elongation zone, wild-type root cells started to rapidly expand accompanied by enlargement of vacuoles (Fig. 6b, c). Meristematic root cells of wild-type roots contained a complex tubular vacuolar network surrounding the nucleus (Fig. 6d, e). Vacuole morphology in mutant roots was severely altered, and appeared as multiple spheres of different sizes distributed within the cell (Fig. 6b–e) in these two zones, similar to reported phenotypes of *fugu5-1 vha-a2 vha-a3* (Kriegel *et al.*, 2015). Based on BCECF-AM staining, the ratio 488/458 indicated vacuole neutralisation (Gao

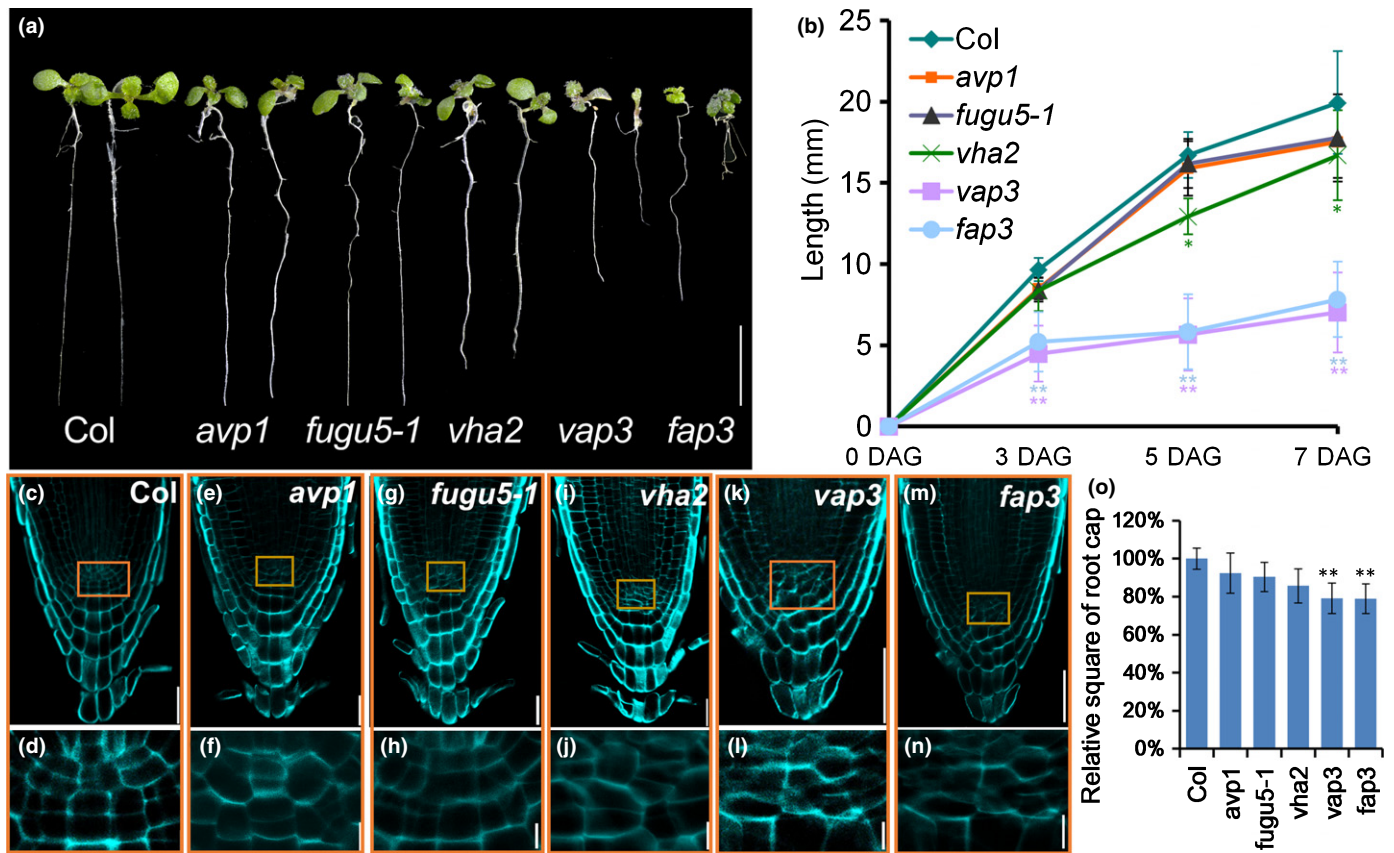


**Fig. 4** Abnormal root development in Arabidopsis mutants *vap3/fap3*. (a) Root length of Col, *avp1*, *fugu5-1*, *vha2*, *vap3* and *fap3*. For a more obvious comparison, the picture shows the seedlings at 9 d after germination (DAG). Graphs represent the typical phenotype of all samples (bar, 5 mm,  $n = 100$  for each line). (b) Statistical analysis of root length. Bars represent the means  $\pm$  SD of three biological replicates ( $n = 30$ ). Asterisks indicate the significant difference (Student's two-tailed  $t$ -test: \*,  $P < 0.05$ ; \*\*,  $P < 0.01$ ). Quiescent centre (QC) region of Col (c, d), *avp1* (e, f), *fugu5-1* (g, h), *vha2* (i, j), *vap3* (k, l) and *fap3* (m, n) (bars, 30  $\mu$ m (c, e, g, i, k, m); 10  $\mu$ m (d, f, h, j, l, n)). Graphs represent the typical phenotype of all samples ( $n = 15$  for each line). (o) Statistical analysis of relative square of root cap. Bars represent the means  $\pm$  SD of three biological replicates ( $n = 10$ ). Asterisks indicate the significant difference (Student's two-tailed  $t$ -test: \*,  $P < 0.05$ ; \*\*,  $P < 0.01$ ).

*et al.*, 2015) in roots of *vap3* (Fig. S6). We further extracted the vacuole from the protoplast (Fig. 6f–k) and found that the diameter of the protoplast and vacuole in *vap3* was reduced compared with those in Col, indicating that vacuole size and morphology were changed in *vap3* embryos.

PIN1 localisation was reported to be regulated by vesicular trafficking (Kleine-Vehn & Friml, 2008). We detected PIN1 localization in wild-type and mutant backgrounds after BFA treatment. Consistent with previous findings for the wild-type background (Kleine-Vehn *et al.*, 2009), PIN1 aggregated into BFA compartments (Fig. 6l–m), but PIN1 protein distribution was largely insensitive to BFA treatment in the mutant background (Fig. 6n–o), suggesting that PIN1 vesicular trafficking may be defective in the *vap3* background and cause abnormal PIN1 polar localisation and auxin distribution.

## Discussion

Our study suggested that AVP1 and VHA-a2/VHA-a3 function in embryo pattern formation and subsequent developmental processes, especially seedling morphogenesis. In our study, null mutants of V-PPase (*fugu5-1* and *avp1*) had basically a normal

development process, PIN1 localisation and auxin content, and these findings were consistent with findings by Kriegel. Vacuolar proton pumps may be involved in vacuole morphology and distribution and have been shown to be associated with early embryo development. A recent study showed that polar distribution of vacuoles plays a role in the first asymmetrical division of the zygote (Kimata *et al.*, 2019). We found that vacuole morphology in *vap3/fap3* embryos at the 1-cell stage was altered compared with the wild-type (Figs 1a–c, 2a–i), consistent with the possibility that the tonoplast proton pump functions in vacuole morphology and distribution affects embryo development. We noted that about 70% (*vap3*) to 77% (*fap3*) of mutant progenies failed to develop to the 1-cell embryo, indicating earlier stage defects in female gametogenesis, fertilisation and/or first zygote division. This finding is consistent with the findings by Kimata and colleagues (Kimata *et al.*, 2019) that vacuole morphology is important for the first division of the zygote. In other words, triple mutants studied here have severe defects in vacuole morphology, leading to the failure of 70–77% zygotes to go through the first cell division. For the 20–30% of the zygotes that did manage to divide, the patterns of cell divisions in subsequent embryogenesis were severely altered, thereby resulting in

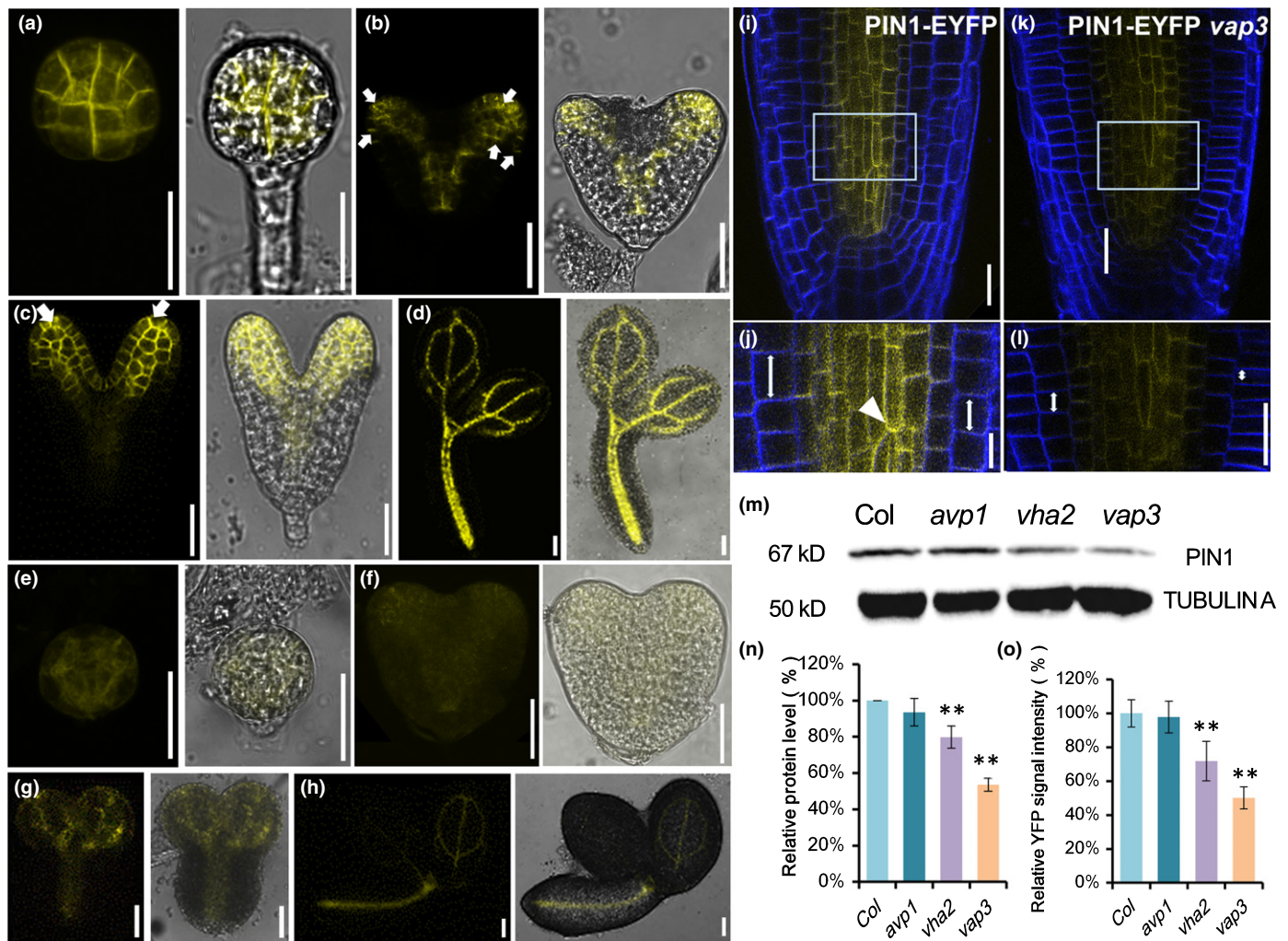


**Fig. 5** Arabidopsis mutant *vap3* has disturbed auxin polar transportation and distribution. (a–h) PIN1 level and localisation in Col (a–d) and *vap3* (e–h) during embryogenesis (bars, 50  $\mu$ m). Graphs represent the average intensity of fluorescence of PIN1 protein in embryos. (i–l) PIN1 level and localisation in Col (i, j) and *vap3* (k, l) seedlings at 5 d after germination (DAG) (Bars, 30  $\mu$ m (i, k); 10  $\mu$ m (j, l)). Arrowhead marks the localisation of PIN1 protein. (m) PIN1 protein level in roots of Col, *avp1*, *vha2* and *vap3*. (n) A quantitative analysis of PIN1 protein levels is shown below and each bar corresponds with the PIN1 band in the blot. Values correspond to the arithmetic means  $\pm$  SD of three biological replicates ( $n = 3$ ). Asterisks indicate the significant difference (Student's two-tailed  $t$ -test: \*\*,  $P < 0.01$ ). (o) Relative PIN1-YFP signal intensity in Col, *avp1*, *vha2* and *vap3*. The data are extracted from normalised mean grey levels of PIN1-YFP in Col, *avp1*, *vha2* and *vap3*. Values correspond to the arithmetic means  $\pm$  SD of three biological replicates ( $n = 20$ ). Asterisks indicate the significant difference (Student's two-tailed  $t$ -test: \*\*,  $P < 0.01$ ).

abnormal pattern formation of the survived embryos. The connection between tonoplast proton pumps and vacuole morphology is logical, as pump activities are the major driving forces for molecular trafficking in and out of the vacuoles, and for controlling turgor pressure and biogenesis of vacuoles.

While defects in early embryo development in the mutant may be a result of altered vacuole morphology and cell division pattern, later defects in seedling development may have been caused by changes in the distribution of PIN1. Vacuole morphology and PIN1 localisation may be linked through cellular pH regulation that controls protein trafficking in the cells (Geldner *et al.*, 2001). Indeed, vacuole morphology and the PIN1-EYFP signal in *vap3* root cells were both altered compared with the wild-type (Figs 5i–l, 6b–e), suggesting a possible connection between vacuole morphology and PIN1 localisation. Lack of proton pump activities directly altered cellular pH homeostasis, leading to higher

pH in vacuole and lower pH in the cytoplasm, which has been proposed to cause abnormal PIN1 localisation (Geldner *et al.*, 2001). As a result, auxin distribution will change and cause further defects in later embryos and in seedling morphology. Defects in *vap3* and *fap3* cotyledons lacking both pumps were similar to those in *pin1-11*, *RPS5A>>PID* (Friml *et al.*, 2004) and *cuc1 cuc2* (Aida *et al.*, 2002), suggesting that these mutants may have severe defects in auxin transport and signalling possibly as a result of changes in PIN1 localisation (Fig. S5b). As a major efflux carrier of auxin, PIN1 plays a critical function in polar auxin transport (Friml *et al.*, 2004; Kleine-Vehn & Friml, 2008). The PIN1 protein has been shown to recycle between intracellular compartments and plasma membrane through vesicular trafficking. The processes that govern endocytosis and exocytosis therefore determine the distribution of the PIN1 protein and consequently auxin transport. Our results illustrated that the abundance and

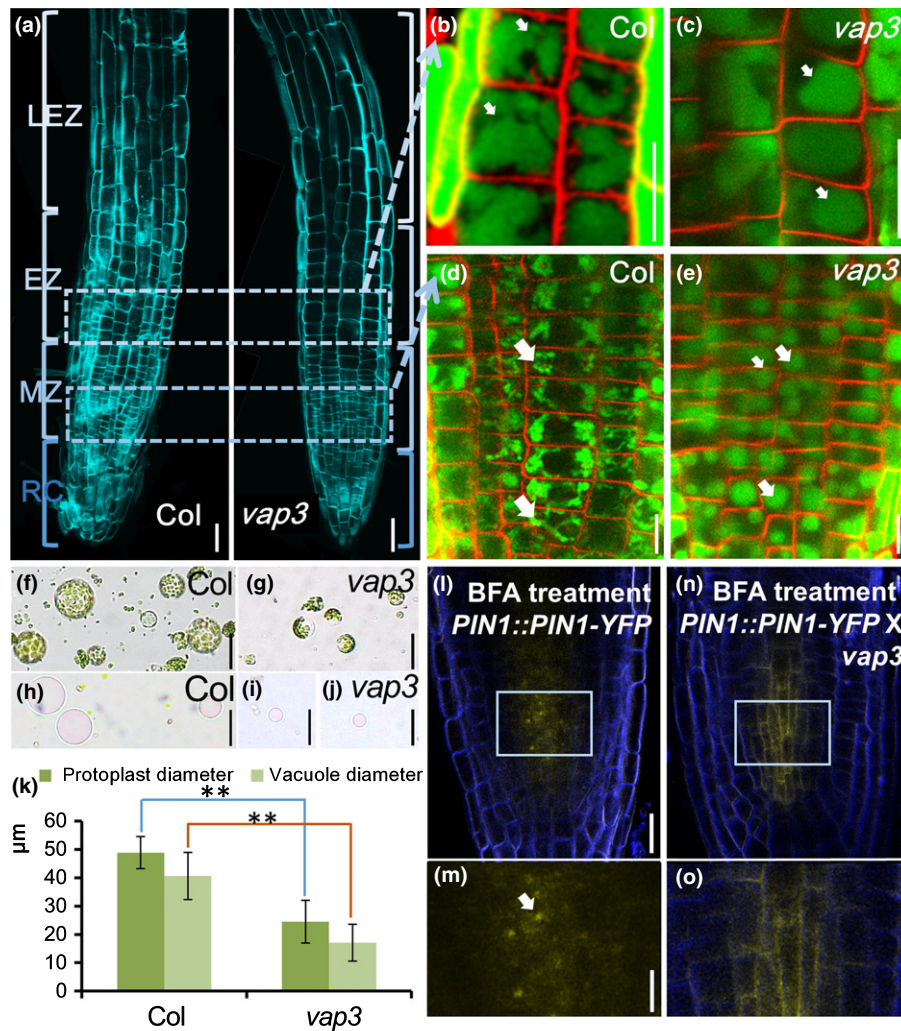


**Fig. 6** Arabidopsis mutant *vap3* has abnormal cell division, vacuole morphology and vesicular trafficking of PIN1 in roots. (a) The root pattern of Col and *vap3* (bars, 100 μm). Roots were stained with FB28 (blue). The shape of vacuoles was monitored in the root elongation zone (b, c), and meristematic zone (d, e) of Col (b, d) and *vap3* (c, e) seedlings at 5 d after germination (DAG). Roots were stained with BCECF (green) and FM4-64 (red). Arrows mark the different vacuoles. Graphs represent the typical phenotype of all samples ( $n = 15$  for each line). Isolated protoplasts of Col (f) and *vap3* (g). Crude vacuoles of Col (h) and *vap3* (i, j) stained with Neutral Red. (k) Statistical analysis of protoplast and vacuole diameters of Col and *vap3*. Bars represent the means  $\pm$  SD of three biological replicates ( $n = 30$ ). Asterisks indicate the significant difference (Student's two-tailed  $t$ -test: \*\*,  $P < 0.01$ ). PIN1 level and localisation in Col (l, m) and *vap3* (n, o) root after BFA treatment (bars, 30 μm (l, n); 10 μm (m, o)). Arrows mark the BFA compartments. Graphs represent the average intensity of fluorescence of PIN1 protein in roots ( $n = 15$  for each line).

exocytosis of PIN1 was disturbed in *vap3* mutants (Fig. 7), and subsequently led to reduced PIN1 abundance in the plasma membrane, suggesting that tonoplast proton pumps may function in PIN1 localisation that in turn controls auxin distribution and embryo/cotyledon development. This finding is consistent with an earlier study on the function of cytosolic subunit C (VHA-C) of V-ATPase (also called DEETIOLATED3, or DET3) (Laxmi *et al.*, 2008), which suggested that DET3 plays a role in trafficking plasma membrane proteins such as PIN2 and BRI1 (Luo *et al.*, 2015). Because loss of DET3 increases the pH in the TGN/EEs, but not the vacuole, authors concluded that DET3 activity controls pH in TGN/EEs, which in turn regulates vesicular trafficking (Laxmi *et al.*, 2008). By contrast, loss of function of both VHA-type and AVP1-type tonoplast proton pumps leads to raised pH of the vacuole (Krebs *et al.*, 2010;

Kriegel *et al.*, 2015). Together with our results here, these findings suggested that vacuolar pH may also be important for intracellular trafficking of plasma membrane proteins such as PIN1, to control auxin transportation and distribution.

In conclusion, the tonoplast proton pumps play essential roles in vacuole morphology and distribution during embryo cell division and embryo pattern formation. At and after the 16-/32-cell embryo stages, PIN1 protein polar localisation becomes a key determinant for further embryo development. The cellular pH (controlled by vacuolar proton pumps) is a key factor for correct trafficking of plasma membrane proteins including PIN1. As Kriegel's research mentioned, a null mutant of V-PPase (*figu5-1*) exhibited no change in developmental processes and vacuole pH. In our opinion, we consider that there are two types of proton pumps at the tonoplast and that they both play a role in

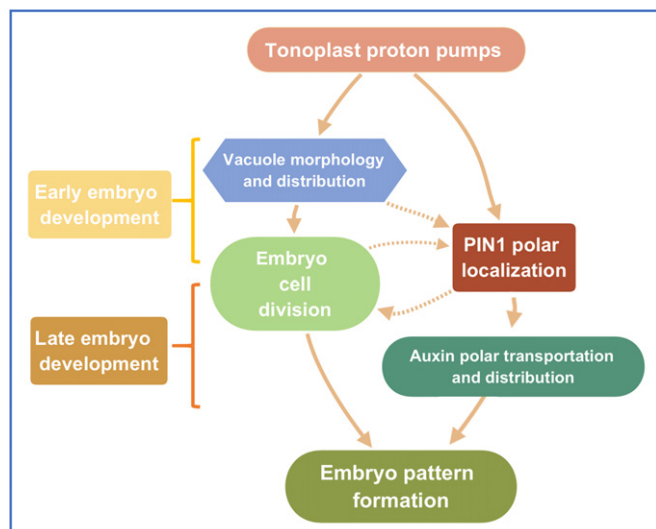


**Fig. 7** The hypothesis model of proton pumps at tonoplast regulating embryo pattern formation in Arabidopsis.

transporting  $H^+$  into the vacuole. If one of these is missing, the other one will also exercise this function (at a partial level). Both the null mutant of V-PPase (*avp1* or *fugu5-1*) and the null mutant of V-ATPases (*vha2*) have the ability to transport  $H^+$  into the vacuole relying on another functional enzyme. But this is not true for *vap3* or *fap3* that has lost the function of both two types of proton pumps resulting in a triple mutant with severe phenotypes. Our hypothesis is similar to the 'share work model' raised in Kriegel's paper (Kriegel *et al.*, 2015). The lack of tonoplast proton pumps therefore would cause severe defects in embryo patterning due to altered vacuolar morphogenesis and pH control (Fig. 7).

## Acknowledgements

We thank Lin Xu (SIPPE, CAS) for donating *pin1-11* seeds, Jian Xu (NUS Centre for BioImaging Sciences) for donating marker lines pPIN1::PIN1-EYFP and DR5::GUS, and Ling Di (Instrumental Analysis Center, Shanghai Jiao Tong University) for advice on confocal imaging. This work was supported by grants from the Natural Science Foundation of China (grant nos. 31761163003 and 31771591 to W-HL), a grant from the National Science Foundation (to SL), the CSC Scholarship (to W-HL), and the Opening Research Projects of National Key Laboratory of Plant Molecular Genetics, SIPPE, CAS (to W-HL).

## Author contributions

W-HL designed the study, performed experiments, analysed data, wrote and modified the manuscript, and acquired funding. SL designed the study, wrote and modified the manuscript, and acquired funding. Y-TJ performed experiments and wrote the manuscript. R-JT performed experiments, Y-JZ helped analysed data. H-WX helped organised the results. AF offered the materials and helped organised the results and the manuscript. All authors agree to be accountable for the content of this paper. SL and W-HL contributed equally to this work.

## ORCID

Ali Ferjani [ID](https://orcid.org/0000-0003-1157-3261) <https://orcid.org/0000-0003-1157-3261>

Wen-Hui Lin [ID](https://orcid.org/0000-0003-0600-6107) <https://orcid.org/0000-0003-0600-6107>

Sheng Luan [ID](https://orcid.org/0000-0002-8375-8276) <https://orcid.org/0000-0002-8375-8276>

Hong-Wei Xue [ID](https://orcid.org/0000-0002-7641-5320) <https://orcid.org/0000-0002-7641-5320>

## References

- Aida M, Vernoux T, Furutani M, Traas J, Tasaka M. 2002. Roles of PIN-FORMED1 and MONOPTEROS in pattern formation of the apical region of the Arabidopsis embryo. *Development* 129: 3965–3974.
- Cipriano DJ, Wang Y, Bond S, Hinton A, Jefferies KC, Qi J, Forgac M. 2008. Structure and regulation of the vacuolar ATPases. *Biochimica et Biophysica Acta (BBA) – Bioenergetics* 1777: 599–604.
- Christensen CA, King EJ, Jordan JR, Drew GN. 1997. Megagametogenesis in Arabidopsis wild type and the Gf mutant. *Sexual Plant Reproduction* 10: 49–64.
- Dettmer J, Hong-Hermesdorf A, Schumacher K. 2006. Vacuolar  $H^+$ -ATPase activity is required for endocytic and secretory trafficking in Arabidopsis. *Plant Cell* 18: 715–730.
- Drozdowicz Y, Rea P. 2001. Vacuolar  $H^+$  pyrophosphatases: from the evolutionary backwaters into the mainstream. *Trends in Plant Science* 6: 206–211.
- Ferjani A, Horiguchi G, Yano S, Tsukaya H. 2007. Analysis of leaf development in fugu mutants of Arabidopsis reveals three compensation modes that modulate cell expansion in determinate organs. *Plant Physiology* 144: 988–999.
- Ferjani A, Segami S, Horiguchi G, Muto Y, Maeshima M, Tsukaya H. 2011. Keep an eye on PPI: the vacuolar-type  $H^+$ -pyrophosphatase regulates postgerminative development in Arabidopsis. *Plant Cell* 23: 2895–2908.
- Friml J, Vieten A, Sauer M, Weijers D, Schwarz H, Hamann T, Offringa R, Jürgens G. 2003. Efflux-dependent auxin gradients establish the apical–basal axis of Arabidopsis. *Nature* 426: 147.
- Friml J, Yang X, Michniewicz M, Weijers D, Quint A, Tietz O, Benjamins R, Ouwerkerk PB, Jung K, Sandberg G *et al.* 2004. A PINOID-dependent binary switch in apical–basal PIN polar targeting directs auxin efflux. *Science* 306: 862–865.
- Galweiler L, Guan C, Muller A, Wisman E, Mendgen K, Yephremov A, Palme K. 1998. Regulation of polar auxin transport by AtPIN1 in Arabidopsis vascular tissue. *Science* 282: 2226–2230.
- Gonzalez N, De Bodt S, Sulpice R, Jikumaru Y, Chae E, Dhondt S, Van Daele T, De Milde L, Weigel D, Kamiya Y *et al.* 2010. Increased leaf size: different means to an end. *Plant Physiology* 153: 1261–1279.
- Geldner N, Friml J, Stierhof YD, Jürgens G, Palme K. 2001. Auxin transport inhibitors block PIN1 cycling and vesicle trafficking. *Nature* 413: 425.
- Gaxiola RA, Li J, Undurraga S, Dang LM, Allen GJ, Alper SL, Fink GR. 2001. Drought- and salt-tolerant plants result from overexpression of the AVP1  $H^+$ -pump. *Proceedings of the National Academy of Sciences, USA* 98: 11444–11449.
- Gao Y, Zhou H, Chen J, Jiang X, Tao S, Wu J, Zhang S. 2015. Mitochondrial dysfunction mediated by cytoplasmic acidification results in pollen tube growth cessation in *Pyrus pyrifolia*. *Physiologia Plantarum* 153: 603–615.
- Herman EM, Li X, Su RT, Larsen P, Hsu H, Sze H. 1994. Vacuolar-type  $H^+$ -ATPases are associated with the endoplasmic reticulum and provacuoles of root tip cells. *Plant Physiology* 106: 1313–1324.
- Kriegel A, Andrés Z, Medzihradsky A, Krüger F, Scholl S, Delang S, Patir-Nebioglu MG, Gute G, Yang H, Murphy AS *et al.* 2015. Job sharing in the endomembrane system: vacuolar acidification requires the combined activity of V-ATPase and V-PPase. *Plant Cell* 27: 3383–3396.
- Krebs M, Beyhl D, Görlich Esther, Al-Rasheid KAS, Schumacher K. 2010. Arabidopsis V-ATPase activity at the tonoplast is required for efficient storage but not for sodium accumulation. *Proceedings of the National Academy of Sciences, USA* 107: 3251–3256.
- Kleine-Vehn J, Friml J. 2008. Polar targeting and endocytic recycling in auxin-dependent plant development. *Annual Review of Cell and Developmental Biology* 24: 447–473.

- Kleine-Vehn J, Huang F, Naramoto S, Zhang J, Michniewicz M, Offringa R, Friml J. 2009. PIN auxin efflux carrier polarity is regulated by PINOID kinase-mediated recruitment into GNOM-independent trafficking in Arabidopsis. *Plant Cell* 21: 3839–3849.
- Kimata Y, Kato T, Higaki T, Kurihara D, Yamada T, Segami S, Morita MT, Maeshima M, Hasezawa S, Higashiyama T *et al.* 2019. Polar vacuolar distribution is essential for accurate asymmetric division of Arabidopsis zygotes. *Proceedings of the National Academy of Sciences, USA* 116: 2338–2343.
- Kurihara D, Mizuta Y, Sato Y, Higashiyama T. 2015. ClearSee: a rapid optical clearing reagent for whole-plant fluorescence imaging. *Development* 142: 4168–4179.
- Li Z, Baldwin CM, Hu Q, Liu H, Luo H. 2010. Heterologous expression of Arabidopsis H<sup>+</sup>-pyrophosphatase enhances salt tolerance in transgenic creeping bentgrass (*Agrostis stolonifera* L.). *Plant, Cell & Environment* 33: 272–289.
- Long JA, Moan EL, Medford JI, Barton MK. 1996. A member of the KNOTTED class of homeodomain proteins encoded by the STM gene of Arabidopsis. *Nature* 379: 66.
- Laxmi A, Pan J, Morsy M, Chen R. 2008. Light plays an essential role in intracellular distribution of auxin efflux carrier PIN2 in Arabidopsis thaliana. *PLoS ONE* 3: e1510.
- Luo Y, Scholl S, Doering A, Zhang Y, Irani NG, Rubbo SD, Neumetzler L, Krishnamoorthy P, Van Houtte I, Mylle E *et al.* 2015. V-ATPase activity in the TGN/EE is required for exocytosis and recycling in Arabidopsis. *Nature Plants* 1: 15094.
- Li J, Yang H, Peer WA, Richter G, Blakeslee J, Bandyopadhyay A, Titapiwantakun B, Undurraga S, Khodakovskaya M, Richards EL *et al.* 2005. Arabidopsis H<sup>+</sup>-PPase AVP1 regulates auxin-mediated organ development. *Science* 310: 121–125.
- Mayer U, Berleth T, Ruiz RAT, Miséra S, Jürgens G. 1993. Pattern formation during Arabidopsis embryo development. *Cellular Communication in Plants*. 93–98.
- Murashige T, Skoog F. 1962. A revised medium for rapid growth and bio assays with tobacco tissue cultures. *Physiologia Plantarum* 15: 473–497.
- Maeshima M. 2001. Tonoplast transporters: organization and function. *Annual Review of Plant Physiology and Plant Molecular Biology* 52: 469–497.
- Nelson N. 2003. A journey from mammals to yeast with vacuolar H<sup>+</sup>-ATPase (V-ATPase). *Journal of Bioenergetics and Biomembranes* 35: 281–289.
- Nishi T, Forgac M. 2002. The vacuolar (H<sup>+</sup>)-ATPases—nature's most versatile proton pumps. *Nature Reviews Molecular Cell Biology* 3: 94–103.
- Neuhaus HE, Trentmann O. 2014. Regulation of transport processes across the tonoplast. *Frontiers in Plant Science* 5: 460.
- Oberbeck K, Drucker M, Robinson DG. 1994. V-type ATPase and pyrophosphatase in endomembranes of maize roots. *Journal of Experimental Botany* 45: 235–244.
- Robert S, Zouhar J, Carter C, Raikhel N. 2007. Isolation of intact vacuoles from Arabidopsis rosette leaf-derived protoplasts. *Nature Protocols* 2: 259–262.
- Sabatini S, Beis D, Wolkenfelt H, Murfett J, Guilfoyle T, Malamy J, Benfey P, Leyser O, Bechtold N, Weisbeek P *et al.* 1999. An auxin-dependent distal organizer of pattern and polarity in the Arabidopsis root. *Cell* 99: 463–472.
- Segami S, Nakanishi Y, Sato MH, Maeshima M. 2010. Quantification, organ-specific accumulation and intracellular localization of Type II H<sup>+</sup>-pyrophosphatase in Arabidopsis thaliana. *Plant & Cell Physiology* 51: 1350–1360.
- Sze H, Schumacher K, Müller ML, Padmanaban S, Taiz L. 2002. A simple nomenclature for a complex proton pump: VHA genes encode the vacuolar H<sup>+</sup>-ATPase. *Trends in Plant Science* 7: 157–161.
- Steinmann T, Geldner N, Grebe M, Mangold S, Jackson CL, Paris S, Gälweiler L, Palme K, Jürgens G. 1999. Coordinated polar localization of auxin efflux carrier PIN1 by GNOM ARF GEF. *Science* 286: 316–318.
- Vernoux T, Kronenberger J, Grandjean O, Laufs P, Traas J. 2000. PIN-FORMED 1 regulates cell fate at the periphery of the shoot apical meristem. *Development* 127: 5157–5165.
- Viotti C, Krüger F, Krebs M, Neubert C, Fink F, Lupanga U, Scheuring D, Boutté Y, Frescatada-Rosa M, Wolfenstetter S *et al.* 2013. The endoplasmic reticulum is the main membrane source for biogenesis of the lytic vacuole in Arabidopsis. *Plant Cell* 25: 3434–3449.
- Xiang D, Datla R. 2011. POPCORN functions in the auxin pathway to regulate embryonic body plan and meristem organization in Arabidopsis. *Plant Cell* 23: 4348–4367.
- Xu J, Hofhuis H, Heidstra R, Sauer M, Friml J, Scheres B. 2006. A molecular framework for plant regeneration. *Science* 311: 385–388.
- Yang Y, Tang RJ, Li B, Wang HH, Jin YL, Jiang CM, Bao Y, Su HY, Zhao N, Ma XJ. 2015. Overexpression of a *Populus trichocarpa* H<sup>+</sup>-pyrophosphatase gene *PrVPI.1* confers salt tolerance on transgenic poplar. *Tree Physiology* 35: 663–677.
- Yang Y, Tang RJ, Mu B, Ferjani A, Shi J, Zhang H, Zhao F, Lan WZ, Luan S. 2018. Vacuolar proton pyrophosphatase is required for high magnesium tolerance in Arabidopsis. *International Journal of Molecular Sciences* 19: 3617.

## Supporting Information

Additional Supporting Information may be found online in the Supporting Information section at the end of the article.

**Fig. S1** Identification of triple mutant *vap3* and *fap3*.

**Fig. S2** Embryogenesis of *avp1* and *vba2*.

**Fig. S3** Defected growth and development in *vap3*.

**Fig. S4** *vap3fap3* has disturbed auxin responses.

**Fig. S5** Auxin-related phenotypes in *vap3fap3* and *pin1-11*.

**Fig. S6** Relative vacuole pH measurement of meristem zone and elongation zone in Col and *vap3* 6-DAG-seedlings roots.

**Table S1** Detection of auxin content of 21-DAG-seedlings of Col, *avp1*, *vba2*, *vap3*.

Please note: Wiley Blackwell are not responsible for the content or functionality of any Supporting Information supplied by the authors. Any queries (other than missing material) should be directed to the *New Phytologist* Central Office.